Low-Pressure Hydrogen Jets from a Single Hole Injector Investigated With 2D Raman and Schlieren Imaging

B. Rüppel[1,2,*], B. Lehnert[1,2], S. Rieß[1,2], E. Berrocal[2,3], M. Wensing[1,2]

1: Friedrich-Alexander-Universität Erlangen-Nürnberg (FAU), Professorship for Fluid Systems Technology, Cauerstraße 4, 91058 Erlangen, Germany
2: FAU, Erlangen Graduate School in Advanced Optical Technologies (SAOT), Konrad-Zuse-Straße 3-5, 91052 Erlangen, Germany
3: Division of Combustion Physics, Department of Physics, Lund University, P.O. Box 118, SE-22100 Lund, Sweden
*Corresponding author: bastian.rueppel@fau.de

Keywords: Raman Imaging, Schlieren Imaging, Hydrogen Jet, Hydrogen Injection, Quantitative Mixture Ratio.

ABSTRACT

This work presents a combined Schlieren and Raman imaging methodology to quantify the spatio-temporal hydrogen–nitrogen mixture ratio of single hole injector jets in an optically accessible chamber at low pressures. The facility accommodates a constant N_2 purge flow, chamber pressures up to 0.6 MPa, and an in-house modified Synerject Strata 1 injector with a single hole cap. Schlieren imaging employs a 640 nm high-speed laser and a high-frame-rate camera to capture jet morphology. For quantitative species mapping, a temporally stretched double-pulse 532 nm Nd:YAG laser of combined energy of 0.8 J traverses the chamber as a light sheet beneath the injector tip. Raman signal collection happens orthogonally and spectrally split to dedicated detection paths for N_2 signals at 607 nm and H_2 signals at 683 nm, each recorded on a low-noise sCMOS camera with 50 µs exposure and an appropriate band pass filter. Stepping the delay between injection and laser constructs time-resolved Raman sequences, averaging 50 shots per frame to overcome single-shot signal limitations. Quantification relies on pixel-wise intensity ratios, where a calibration factor incorporates the species-dependent Raman scattering cross sections and the wavelength dependencies of the full detection chain. The calibration matrix is derived from known H_2/N_2 mixtures at two pressure levels that yield values close to prior point-measurement benchmarks. Rigorous image processing includes geometric transformation for pixel overlap, subtraction of laser-independent dark images acquired between laser pulses, and laser-induced background removal by subtraction of isolated background images taken in helium fills. Interpolation and median filtering mitigate near-zero divisions. Schlieren images provide clear jet outlines and facilitate penetration and cone-angle tracking but lack direct physical meaning for the apparent boundary. In contrast, Raman mapping reveals a mixture-fraction gradient at the jet edge and captures nitrogen entrainment toward the core, with uncertainty increasing where N_2 counts approach zero. Non-uniform illumination limits the region of good signal-to-noise ratio, because one beam of the double-pulse is diverging and thereby restricting how close illumination can come to the injector. Example cases with comparable pressure ratios (0.9 MPa H_2 into 0.3 MPa N_2 for Schlieren; 1.6 MPa H_2 into 0.5 MPa N_2 for Raman) show good agreement in overall jet shape. Raman imaging enables quantitative, time-resolved mixture-field data at moderate pressures for model validation. Planned improvements target light-sheet uniformity and placement, comprehensive uncertainty analysis for various evaluation strategies and a systematic parametric study of jets under a variation of pressure ratios.

1. Introduction

Hydrogen fueled internal combustion engines are supposed to be an addition to battery electric and fuel cell powertrains on the path to climate-neutral transportation and especially interesting in off-highway applications (Onorati et al., 2022). The technical process of mixture formation of hydrogen and air can thereby follow various principles, e.g. direct or port fuel injection. Unlike liquid fuel sprays, hydrogen forms a gaseous jet. This limits the diagnostic tools available to developers and researchers to experimentally characterize the processes involved. The Schlieren technique seems to be the method of choice for jet visualization in many recent publications (Payri et al., 2024; Peters et al., 2024; H. Wu et al., 2025). However, in 2009 Bräuer and Leipertz reported on the application of 2D Raman imaging to hydrogen injection in a optical accessible chamber (Braeuer & Leipertz, 2009) and Engel et al. in a transparent engine (Engel et al., 2009). The latter study also used laser-induced fluorescence (LIF). This technique has the constraint of requiring tracer molecules mixed into the hydrogen. Engel et al. used triethylamine and trimethylamine. The second is beneficial, because it is gaseous under ambient conditions. However, more recently, Leick et al. used the liquid acetone as an LIF tracer in hydrogen (Leick et al., 2023). In 2023, a group of the Clean Energy Research Platform at King Abdullah University of Science and Technology reestablished 2D Raman together with Rayleigh imaging (B. Wu et al., 2023).

Raman scattering is an inelastic form of light scattering at molecules. The scattered light is of a wavelength different from that of the incident light. The magnitude of the shift of wavelength is characteristic for certain molecules. This allows to evaluate the Raman scattered light in spectroscopic measurement techniques and obtain the chemical composition of the scattering volume. Compared to Schlieren imaging, which visualizes gradients of the refractive index, Raman spectroscopy benefits from quantitative results, but especially in gases it is challenging because of weak signals. The signal intensity of a certain transition is a function of a set of the experimental conditions as given in equation 1.

$$I \propto n \cdot \sigma \cdot \Omega \cdot k \cdot l \cdot I_0 \tag{1}$$

The number density of potential scatterers n, the scattering cross section σ, the detection solid angle Ω, a device factor k, the interaction length l and the excitation intensity I_0 all act linearly on the scattered intensity I that a detector registers.

Raman scattering cross sections describe the probability of scattering events. They are properties of the chemical species and on the order of as low as 10^{-31} cm^2, making Raman transitions rare in comparison to Rayleigh scattering or LIF for example (Fenner et al., 1973).

On top of that, the number density of possible scatterers is small in gases. Increasing the pressure is therefore a way of enhancing Raman signals. The aforementioned studies by Braeuer & Leipertz (2009) and B. Wu et al. (2023) inject into an ambient of 0.95 and 1.0 MPa, respectively. However, Wu

et al. still describe the limitation of the method by comparing the 2D imaging to 1D experiments that have higher accuracy (B. Wu et al., 2024).

In this study, we aim to establish a 2D Raman imaging experiment that allows for quantification of hydrogen jets at lower pressures. We use Schlieren images as the reference to compare the outline of the plume.

2. Experimental Setup

2.1. Constant volume continuous flow chamber and injector

All experiments take place in a constant volume continuous flow chamber. On three sides it offers optical access through anti-reflection coated windows. The windows have an aperture diameter of 40 mm. The top of the chamber holds the injector with its axis right in the center and two further gas inlets next to it. These inlets are for purging and filling the chamber and are connected to a gas mixing setup consisting of one mass flow controller for hydrogen and one for nitrogen. Apart of those, it is also possible to fill the chamber with helium. On the bottom side, a gas outlet leads to a pressure regulator. There are no heaters and all experiments happen at room temperature.

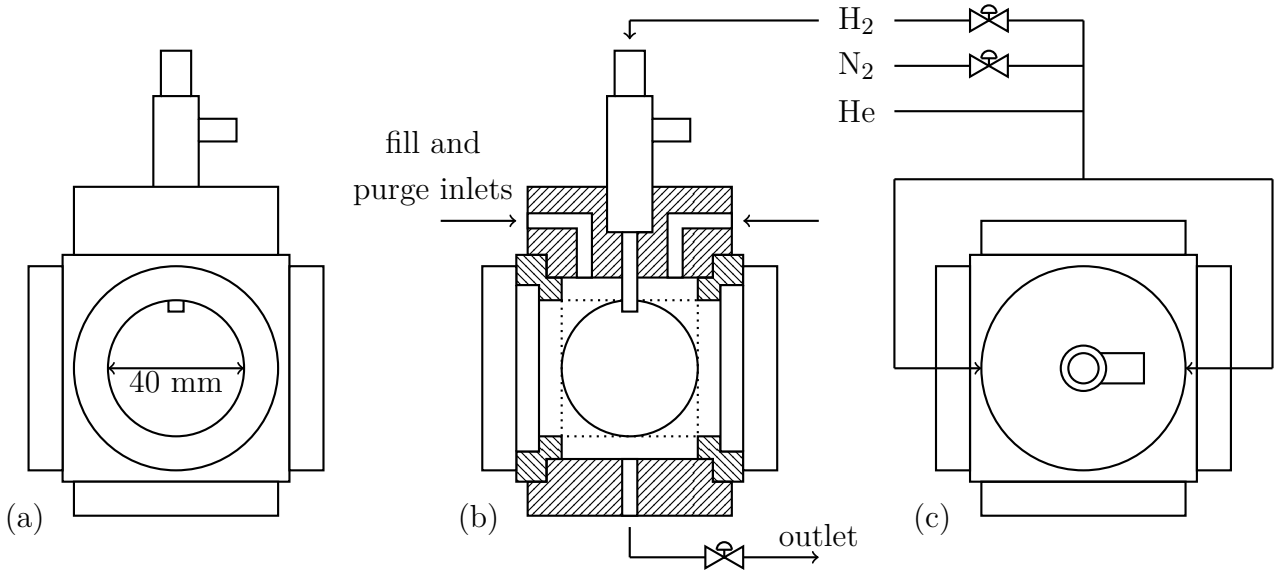


Figure 1. Schematic of the constant volume continuous flow chamber. (a) Front view. (b) Cross-sectional view of the main body and top and bottom flanges for visualization of gas channels. (c) Top view.

For calibration measurements, we set up the mass flow controllers for known ratios of hydrogen and nitrogen. For injection experiments, we fill the chamber with pure nitrogen under pressures of up to 0.6 MPa and constantly purge with a flow rate of 5 nl·min^{-1}. The injection pressure is chosen accordingly with variation of pressure ratios. It is directly set on the gas cylinder.

The base of the injector is an outward-opening valve type Synerject Strata 1. We modified it by adding an in-house single hole cap. A scientific Genotec energizing unit drives the injector.

2.2. Schlieren Imaging Setup

A lens of 200 mm focal length collimates the light from a high-speed 640 nm Laser (Cavilux HF) for the Schlieren imaging. Behind the chamber, another lens of 200 mm focal length focuses onto the tip of a needle that blocks off non-diverted beams. A Photron SA1.1 high-speed camera with a Zeiss Makro-Planar 2/100mm camera lens at maximum aperture opening records the remaining light. Camera and Laser timing are synchronized by the camera software, a Quantum Composer pulse generator triggers the start of injection and recording.

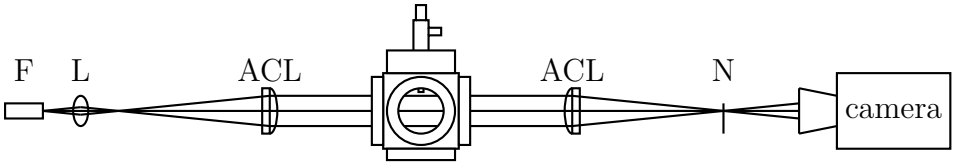


Figure 2. Schematic of the Schlieren imaging setup. F: Optical fiber outlet, L: Spherical lens $f = 25$ mm, ACL: achromatic doublet $f = 200$ mm, N: needle tip (functioning as knife edge).

2.3. Raman Imaging Setup

The excitation source for the Raman images is a pulsed Nd:YAG laser from InnoLas, emitting frequency-doubled 532 nm light. At a rate of 5 Hz it produces a double-pulse with a combined energy of 0.8 J measured with a gentec-eo energy meter. The two pulses of the double-pulse are spaced by 1 µs and are 10 ns long each. First, we use a pulse stretcher to extend the duration in order to prevent window breakdown. The stretcher has a 40/60 beam splitter, where we guide the larger share through a loop of approx. 3 m length.

We then control vertical polarization and shape the beam of the stretched pulse into a light sheet with a positive cylindrical lens of 500 mm focal length. It passes through two opposite windows of the chamber at a distance beneath the injector tip with the focal line right below its axis.

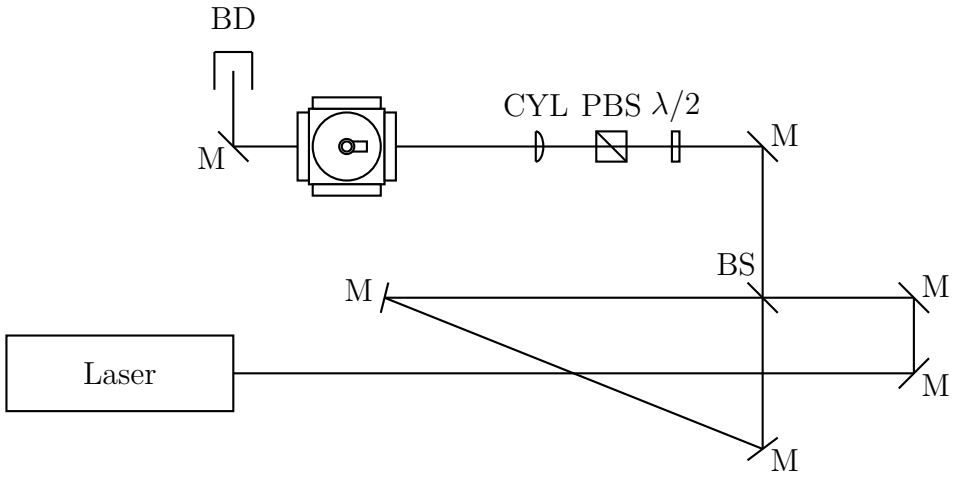


Figure 3. Schematic of the excitation laser path for Raman imaging. M: flat mirror, BS: 40/60 beam splitter, $\lambda/2$: half-wave plate, PBS: polarizing beam splitter cube, CYL: cylindrical lens $f = 500$ mm, BD: beam dump.

Signal detection happens under an angle of 90° through a perpendicular window. First, an achromatic doublet of 75 mm focal length collects the signals. A 532 nm notch filter removes contributions from Rayleigh scattering. In the following, a dichroic mirror with cut-on at 638 nm separates N_2 from H_2 Raman signals, which each reach a set of a Schneider Onyx F0.95/25 mm lens, bandpass filter and Andor Zyla 5.5 sCMOS camera. The center wavelengths of the bandpass filters are 610 nm for N_2 signals peaking at 607 nm (Thorlabs) and 685 nm for H_2 signals at 683 nm respectively (Semrock). Figure 4 illustrates the optical setup used for the detection of signals.

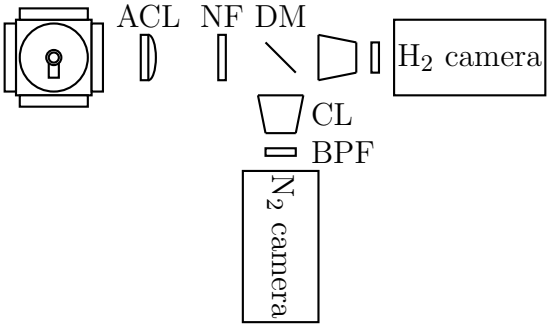


Figure 4. Schematic of Raman signal detection setup. ACL: achromatic doublet $f = 75$ mm, NF: notch filter, DM: dichroic mirror, CL: camera lens, BPF: band pass filters for N_2 and H_2 Raman lines mounted between CL and sensors.

Adding the achromatic doublet close to the chamber serves the purpose of increasing the solid angle of detection Ω and maximizing the signal yield. Numerical considerations justify the choice of its position and focal length and showed that there is a strong benefit, but the achievable optimum will however be limited by the choice of camera lens.

The Zyla camera offers high quantum efficiency and low noise. We choose an exposure time of

50 µs. Per injection we take one image on each camera and derive mixture ratios from the comparison. For a full video, we adjust the timing between start of injection and laser pulses in steps. All trigger signals are controlled by a Quantum Composer pulse generator.

3. Raman Signal Evaluation

The ultimate goal of the Raman imaging experiment is to quantify the local mixture ratio between hydrogen and nitrogen. Referring back to equation 1, the benefit of calculating the ratio lies in canceling out the constant terms. This yields the equation

$$\frac{I_{H_2}}{I_{N_2}} = c \cdot \frac{n_{H_2}}{n_{N_2}}, \tag{2}$$

that we apply to the intensity ratios as recorded by the cameras. The calibration factor c includes two contributions. On one hand, there is the ratio between the Raman scattering cross sections of Hydrogen and Nitrogen. The term relative Raman scattering cross section, where Nitrogen is also chosen as the basis, is a common concept to give the cross section of any species in literature. It is itself dependent on the excitation wavelength. For hydrogen, different values are present in the literature. We addressed this issue in a previous work (Rüppel et al., 2024).

On the other hand, there are wavelength dependencies in losses and efficiencies of the detection. This means that k in equation 1 is not the same for the nitrogen and hydrogen signals and does not cancel out. Examples are the quantum efficiency of the camera or the transmission characteristic of the optical filters.

Experiences from point-wise Raman gas composition measurements advice to combine all influences into one single calibration factor c that we determine experimentally by filling the chamber with known mixture ratios of hydrogen and nitrogen, capturing the Raman intensities and solving equation 2 for the calibration factor. For point measurements, this yields a scalar result, e.g. $c = 2.34$ in the case of the setup presented in earlier work (Rüppel et al., 2024). For the imaging however, there can also be spatial dependencies and there will be a scalar factor for each pair of corresponding camera pixels, that finally means a calibration matrix.

It is crucial to ensure pixel-by-pixel alignment of the field of view of both cameras before evaluating the intensity ratio. We apply a slight geometric transformation on the raw images of the hydrogen camera in MATLAB®, where we also perform all further operations of the evaluation. Figure 5 shows the agreement between an unaltered view of the nitrogen camera with the result of the transformation on the hydrogen camera.

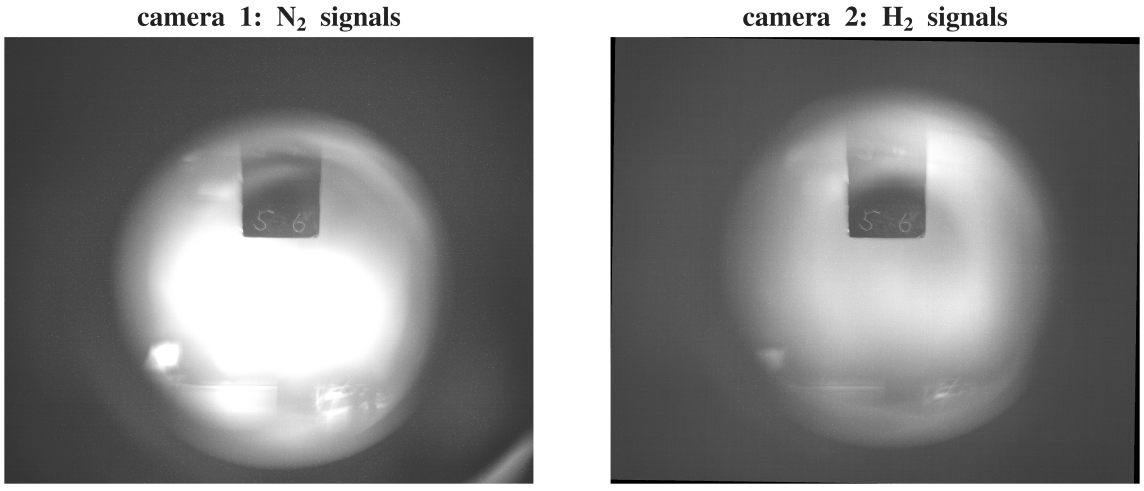


Figure 5. Field of view after geometric transformation. The left image shows the unaltered view of camera 1 capturing N_2 Raman signals. The right image shows the view of camera 2 (H_2 signals) after the transformation.

On each pixel, counts from different sources overlay the Raman signals. They include a flat-field bias, dark current, stray light and laser-induced backgrounds like fluorescence. Before calculating intensity ratios, they need to be removed. For that, we determine two corrections per camera, one with the isolated laser-induced background and one with laser-independent influences.

For the latter, that we call D for dark image, the cameras record an image in the absence of laser light. This could easily be done before conducting an experiment, but the cameras show non-uniformity in a fixed-pattern manner that changes over time. Therefore, it is better to determine D in close temporal proximity to images carrying signal. We record it in between two laser pulses.

The laser-induced background B needs to be measured with the laser pulse during an exposure, but without simultaneously detecting Raman signals. We realize that by filling the chamber with helium, which is not Raman active. This cannot be done during injection experiments. The images taken in helium contain counts from B and D whereas also here we subtract additional dark images taken between laser pulses. If subtraction yields negative pixel counts, those values are set to zero.

To sum up the evaluation process, we first correct the individual signals by subtracting the laser-induced and laser-independent background contributions. Then, we apply geometric transformation to the hydrogen image to ensure spatial overlap and finally, we calculate the mixture ratio from the intensity ratio under incorporation of the calibration factor.

In the end, we replace large values originating from division by pixel counts close to zero with linear interpolation and apply a median filter.

4. Results

4.1. Schlieren Imaging

The Schlieren images are of proper contrast and allow the extraction of shape features like cone angle and penetration depth over time. At this point, the time series in figure 6 will only serve as an orientation for the Raman results. It shows the propagation of a jet with 0.9 MPa hydrogen pressure into 0.3 MPa nitrogen atmosphere as raw, single shot images recorded with 5400 fps.

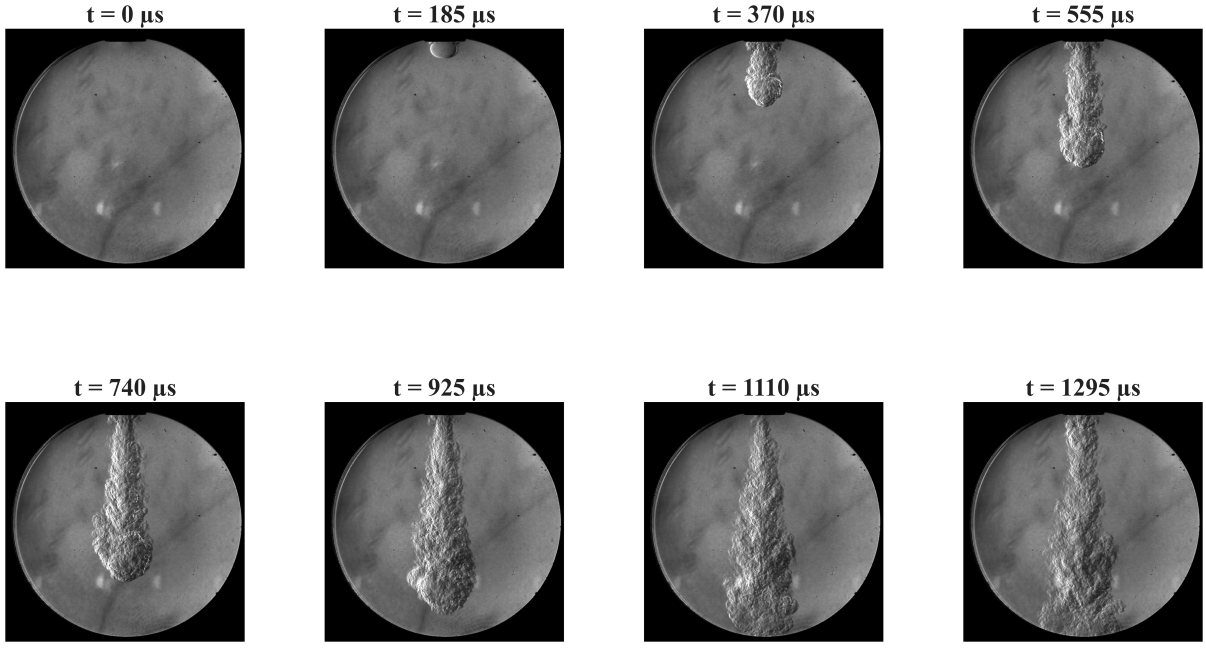


Figure 6. Sequence of raw Schlieren images of an injection with 0.9 MPa hydrogen pressure and 0.3 MPa ambient pressure at 5400 fps. The window diameter is 40 mm.

In the Schlieren depiction, the jet shows a clear and well-defined outer boundary that is linked to a certain unknown gradient in refractive index. Furthermore, the signal is an accumulation along the full light path. As a consequence, there is no real physical meaning assigned to that boundary.

4.2. Raman Imaging

The calibration experiments in atmospheres of known composition follow a good linearity as postulated in equation 2. Figure 7 shows the values of the final matrix of calibration factors c under incorporation of in total seven measured mixtures at two pressure levels: 80/20, 60/40, 40/60 and 20/80 at 0.3 MPa as well as 75/25, 50/50 and 25/75 at 0.5 MPa.

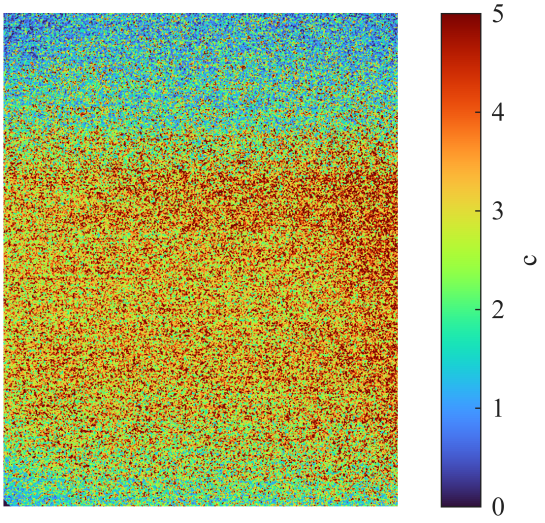


Figure 7. Calibration factor c per pixel for Raman evaluation.

The upper quarter and lower edge of the image show notably lower values. These regions are where the excitation intensity of the laser light sheet is insufficient. One of two laser pulses is diverging so that its light sheet is higher than the other. Its upper boundary limits how close the excitation can approach the injector tip, but its irradiance cannot produce Raman signals with good signal-to-noise ratio. The same pattern is visible in all following images.

In the well illuminated region, most pixels show a calibration factor close to the aforementioned point measurement case, where $c = 2.34$. This is expected, because the Raman scattering cross section is the dominating contribution. To the right however, there is a tendency to larger values. This supports the expectation of positional, spectral dependencies in the detection efficiency. At the same time, the small scales on which we find strong local changes are problematic. The expectation would suggest smoother overall structures. The reason behind this could be that the data foundation is not large enough and too noisy. Future work will aim for improvements on this aspect, either through extended experiments or additional, more analytical post-processing.

Figure 8 shows the propagation of a jet of 1.6 MPa hydrogen into 0.5 MPa nitrogen. Despite the pressure levels being different from the Schlieren case seen in section 4.1, the jets can be compared because the pressure ratio is the relevant property to the process. Here it is 3.2, similar to the pressure ratio of 3 in the Schlieren case.

Each image contains combined information of 50 injections, because the signals of single shots are insufficient. The timing between laser illumination and electronic start of injection increases stepwise after 50 repetitions. Also here, in the upper quarter and on the lower edge of the image, the signal quality suffers from aforementioned light sheet conditions. Still it is possible to localize the leading edge.

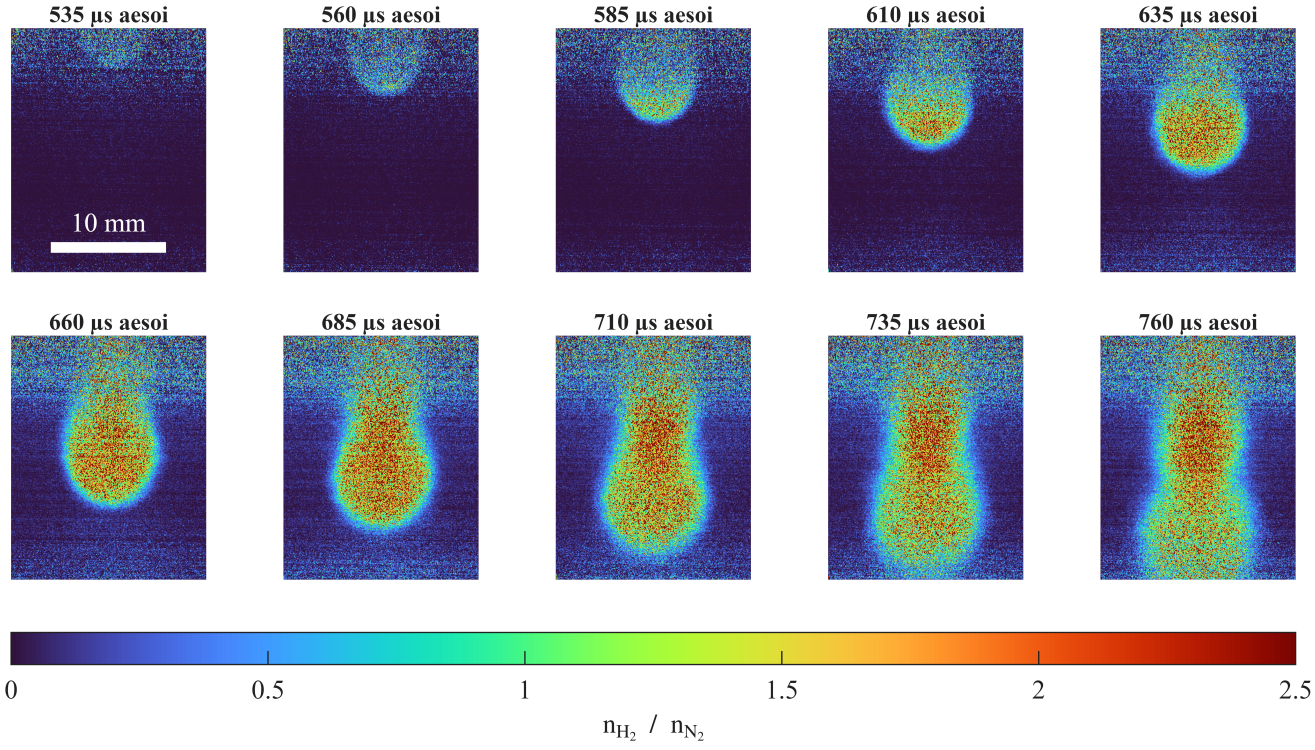


Figure 8. Sequence of Raman images of an injection with 1.6 MPa hydrogen pressure and 0.5 MPa ambient pressure. Each image is an average of 50 injections and the time after electronic start of injection (aesoi) increases stepwise.

The overall shapes agree well, but in contrast to the Schlieren images in figure 6, here there is no sharp boundary of the jet, but rather a moderate gradient. There are two independent reasons to this. One is the step of averaging 50 injections. Shot-to-shot variations of the morphology result in blurring of the mean image. The same happens when we average Schlieren images in equal manner, e.g. before determining the cone angle or penetration depth. At the same time, there is a real physical gradient of mixture ratios due to entrainment and diffusion that Raman imaging can detect. That means with this technique, a physical meaning can be assigned to the gradient in the image and the results regarding cone angle and penetration will depend on the chosen threshold: The lower the mixture ratio we define as the outer boundary, the bigger the angle and penetration will be. We will design upcoming experiments in order to isolate the real, physical gradient from the influences that the mathematical treatment introduces.

Figure 9 shows a detailed view of the image at 685 µs after electronic start of injection combined with a line plot perpendicular to the jet axis.

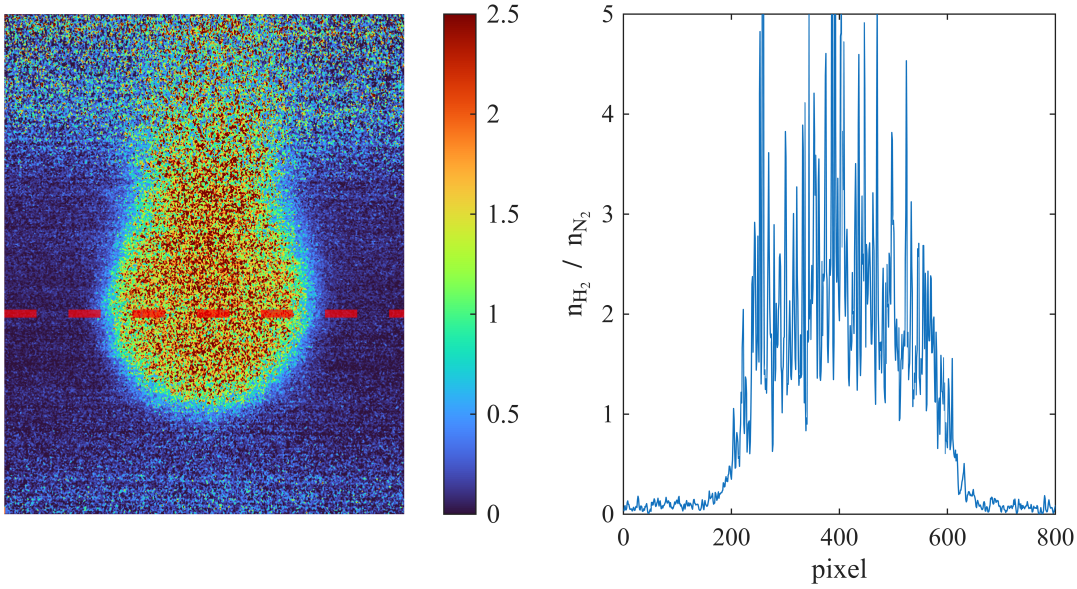


Figure 9. Detail view of the Raman result for timestep 685 µs after electronic start of injection. Image on the left and line plot along the red, dashed indicator of the left panel on the right.

In the line plot on the right panel, the values are the vertical mean of five neighboring horizontal lines. The red, dashed indicator marks their position in the left panel. Here it is noteworthy, that in the core of the jet, the results of mixture ratios become very uneven. There is a small share and number density of nitrogen and the average pixel counts of the nitrogen signals approach zero. The consequences are a bad signal-to-noise ratio on one hand and problems through division by zero on some pixel on the other. Nevertheless, the results still show the entrainment of nitrogen into the core with a maximum on the center axis as expected.

5. Outlook

Future work will progress along three different aspects. First of all, there are necessary improvements to the experimental setup to be implemented. Foremost, this means aligning both laser beams in non-diverging fashion and closer to the height of the injector tip.

The second branch will be about in-depth assessment of the quality of the obtained results with special regard to the image processing. This means analysis of accuracy and precision, error propagation and estimation of uncertainties as well as comparison to theory. Furthermore, this covers testing alternative approaches of quantification logic.

Thirdly, we will conduct an extensive study on the jet behavior under variation of pressure ratios and pressure levels for an industrially relevant injector. Schlieren images will play an important role in testing self-similarity of the jets to justify the averaging we need to do for Raman.

6. Conclusions

We present a new experimental setup that allows the quantification of the mixture formation in hydrogen jets. The application of Raman imaging is now possible at lower pressure levels than demonstrated in the referenced studies.

Comparison of the Raman results to high-speed Schlieren images shows agreement in the morphology and outline shape of the jet. The benefit of Raman imaging lies in the measurement of hydrogen to nitrogen mixture ratios. Due to diffusion and entrainment, there is some nitrogen present in the core of the jet and a moderate gradient towards the ambient. The quantification enables us to determine cone angles and penetration depths with a physical meaning by choosing threshold values accordingly making this more valuable than pure Schlieren measurements.

The Raman imaging requires a comparably high experimental effort, because the signal intensities in gases are small, especially in low pressures. Part of our approach is a tailor-made constant volume continuous flow chamber, optimized for minimal optical losses. Still, it is necessary to average multiple injections. We can not yet state a substantial estimate of the precision that we finally reach. The uncertainties will dictate the required number of repetitions. A corresponding analysis will be subject to upcoming work alongside further experimental improvements and a parametric study of jet behavior.

Acknowledgments

The authors gratefully acknowledge funding of the Erlangen Graduate School in Advanced Optical Technologies (SAOT) by the Bavarian State Ministry for Science and Art.

The authors gratefully acknowledge funding by the Bavarian Ministry of Economic Affairs, Regional Development and Energy as part of the program “Hydrogen Mixture Formation in Off-Highway Applications” under funding code 45-6665n/132/2-MIA-2210-0011 and by the Bavarian Research Foundation (Bayerische Forschungsstiftung) under grant number AZ-1606-23 within the project “InnoBurst”.

Nomenclature

B	Laser-induced background
c	Calibration factor
D	Dark image
f	Focal length in m
I	Intensity

k	Device factor
l	Interaction length in m
n	Number density in m^{-3}
t	Time in s
σ	scattering cross section in m^2
Ω	Solid angle of detection in sr

References

Braeuer, A., & Leipertz, A. (2009). Two-dimensional raman mole-fraction and temperature measurements for hydrogen-nitrogen mixture analysis. *Applied optics*, *48*(4), B57-64. doi: 10.1364/AO.48.000B57

Engel, S. R., Koch, P., Braeuer, A., & Leipertz, A. (2009). Simultaneous laser-induced fluorescence and raman imaging inside a hydrogen engine. *Applied optics*, *48*(35), 6643–6650. doi: 10.1364/AO.48.006643

Fenner, W. R., Hyatt, H. A., Kellam, J. M., & Porto, S. P. S. (1973). Raman cross section of some simple gases. *Journal of the Optical Society of America*, *63*(1), 73. doi: 10.1364/JOSA.63.000073

Leick, P., Jochmann, P., Geiler, J. N., Stapf, K. G., Mansbart, M., & Potenza, M. (2023). Analysis of fuel injection and mixture formation in hydrogen engines. In *12th meeting injection and fuels.*

Onorati, A., Payri, R., Vaglieco, B. M., Agarwal, A. K., Bae, C., Bruneaux, G., … Zhao, H. (2022). The role of hydrogen for future internal combustion engines. *International Journal of Engine Research*, *23*(4), 529–540. doi: 10.1177/14680874221081947

Payri, R., Novella, R., Nasser, K. I., & Bori-Fabra, O. (2024). Spray characterization of direct hydrogen injection as a green fuel with lower emissions. *Energies*, *17*(10), 2405. doi: 10.3390/en17102405

Peters, M., Maes, N., Dam, N., & van Oijen, J. (2024). Characterizing and visualizing the direct injection of hydrogen into high-pressure argon and nitrogen environments. *International Journal of Hydrogen Energy*, *66*(7), 304–315. doi: 10.1016/j.ijhydene.2024.04.054

Rüppel, B., Lehnert, B., Weiß, L., & Wensing, M. (2024). Long-term continuous gas diagnostics for fuel cell systems: Development of an automatized raman metrology. *Proceedings of the 21st International Symposium on Application of Laser and Imaging Techniques to Fluid Mechanics*.

Wu, B., Sharma, P., Yu, T., Palombi, L., Wu, H., Ben Houidi, M., … Magnotti, G. (2023). High-speed 2-d raman and rayleigh imaging of a hydrogen jet issued from a hollow-cone piezo injector.

In B. Wu et al. (Eds.), *Sae technical paper series.* SAE International400 Commonwealth Drive, Warrendale, PA, United States. doi: 10.4271/2023-24-0019

Wu, B., Wu, H., Houidi, M. B., Sharma, P., Cenker, E., AlRamadan, A. S., … Magnotti, G. (2024). High-speed 1-d and 2-d raman scattering measurement for quantitative characterization of transient hydrogen jets. *Proceedings of the Combustion Institute*, *40*(1-4), 105417. doi: 10.1016/j.proci.2024.105417

Wu, H., Ben Houidi, M., Almatrafi, F., Wu, B., Du, J., Magnotti, G., & Roberts, W. L. (2025). Hydrogen jet characteristics with an outwardly opening piezo injector. *Physics of Fluids*, *37*(3). doi: 10.1063/5.0252859